scientific reports

Check for updates

OPEN

In silico evaluation of the anti *Helicobacter pylori* activity of selected bioactive compounds from *Aloe vera*

Uwem Okon Edet[1,2]✉, Edema Enogiomwan Imalele[3], Wafa Ali Eltayb[4,5], Glory Bebia[6], Maaweya E. Awadalla[7], Aniekan-Augusta Eyo[6], Reham M. Alahmadi[8], Bassey Edet[2], Francisca Nwaokorie[9] & Mohnad Abdalla[10]✉

Helicobacter pylori **causes peptic ulcer, which is estimated to affect about half of the human population. Current treatments present with adverse side effects, and increasing antibiotic resistance have intensified the search for alternative therapeutic agents. Aim: This study explores the inhibitory potential of selected bioactive compounds of *Aloe vera* against *H. pylori* neutrophil-activating protein (NAP) using an in-silico approach. Methods: Molecular docking, simulation (300 ns), ADMET (absorption, distribution, metabolism, excretion and transportation) predictions and density function theory (DFT) were carried out using standard protocols with the co-crystal or native ligand used as control. Results: Docking results identified aloesin as the top candidate (-7.4 kcal/mol), followed by aloe-emodin and chrysophanic acid (-6.4 kcal/mol) and esculetin (-6.3 kcal/mol), all outperforming the control ligand (-4.3 kcal/mol). Key receptor-ligand interactions involved amino acids residues, including Ser135, Glu46, and Tyr99, essential for binding stability. Molecular dynamics simulations confirmed complex stability, with RMSD values ≤ 4 Å. RMSF analysis highlighted fluctuations at residues 30, 80/85, and 140, while contact analysis revealed the significance of water bridges and hydrogen bonds. ADMET profiling revealed that all the ligands complied with the Lipinski rule of five and exhibited high intestinal absorption values. Our ranking of the ligands using the docking affinities and RMSD values showed that chrysophanic acid and esculetin were the best ligands. The DFT evaluation showed that esculetin was the most reactive of all the ligands indicated by its least energy score. These findings suggest that aloesin, chrysophanic acid and esculetin could serve as promising alternatives for *H. pylori* treatment. However, further in vitro and in vivo studies are needed to validate their therapeutic potential.**

Keywords *Aloe vera*, In-silico, Ulcer, Simulation, Therapeutics, Docking, ADMET

Helicobacter pylori (*H. pylori*) is a highly mobile, curved, Gram-negative bacterium that colonises the human gastroduodenal mucosa[1]. This bacterium has unique microbiological characteristics, which enable it to survive in extreme environments, including the acidic conditions of the stomach. The primary mode of transmission is oral-faecal, through contaminated food and water[2]. *H. pylori* infection affects approximately half of the world's population, posing a significant public health concern, and its prevalence continues to rise[3]. The Neutrophil-

[1]Regional Laboratory for Animal Influenza and Transboundary Animal Diseases, National Veterinary Research Institute (NVRI), Vom 930101, Plateau State, Nigeria. [2]Department of Biological Science (Microbiology Unit), Arthur Jarvis University, Akpabuyo, Cross River State, Nigeria. [3]Department of Zoology and Environmental Biology, Faculty of Biological Sciences, University of Calabar, PMB1115, Calabar, Cross River State, Nigeria. [4]School of Medicine, Qilu Institute of Technology, Jinan, Shandong, PR China. [5]Biotechnology Department, Faculty of Science and Technology, Shendi University, Nher Anile, Shendi 11111, Sudan. [6]Department of Medical Bacteriology, Virology & Mycology, Faculty of Medical Laboratory Science, University of Calabar, PMB1115, Cross River StateCalabar, Nigeria. [7]Research Center, King Fahad Medical City, Riyadh, Saudi Arabia. [8]Department of Botany and Microbiology, College of Science, King Saud University, P.O.Box 22452, Riyadh 11495, Saudi Arabia. [9]Department of Medical Laboratory Science, College of Medicine, University of Lagos, Lagos, Lagos State, Nigeria. [10]Pediatric Research Institute, Children's Hospital Affiliated to Shandong University, Jinan 250022, China. ✉email: uwemedet27@gmail.com; mohnadabdalla200@gmail.com

Activating Protein (NAP) of *H. pylori* is a key virulence factor that contributes to increased inflammation and oxidative stress in the stomach, which leads to the development of ulcers[4,5]. The NAP activates the neutrophils prompting them to produce reactive oxygen species (ROS) and adhere to endothelial cells, thereby increasing the inflammatory response and oxidative damage to gastric tissues[4,5]. In addition, NAP protein also stimulates the mast cells and monocytes and, in the process, enhances their pro-inflammatory and pro-oxidant activities[4,5]. Collectively, these inflammatory and oxidative stress reactions induced by the NAP of *H. pylori* alter the gastric mucosal barrier, leading to tissue injury and the development of peptic ulcers and their characteristic symptoms[4,5].

Peptic ulcers are treatable, and several pharmacological options are currently in use[6]. Current treatment typically involves antibiotics, acid suppression, and lifestyle modifications (dieting)[6,7]. However, the main route for the management of ulcers is via the use of antibiotics and proton pump inhibitors, whose ultimate aim is the eradication of the bacterium[6]. Other options include the discontinuation of Non-Steroidal Anti-Inflammatory Drugs (NSAIDs) and reduction of gastric acid secretion to promote healing[6]. The continued increase in the prevalence of *H. pylori* infection highlights the issues with existing medication. Resistance of *H. pylori* to existing antibioticshave been reported[8–10]. Existing treatment, especially the triple therapy that combines antibiotics and proton pump inhibitors, currently presents with declining success rates over the past decade, largely driven by the evolution of resistance by the bacterium[8–10]. Furthermore, available medications such as the bismuth quadruple therapy require patients to take four different medications multiple times daily for either 10 or 14 days[11,12]. Taking multiple medications can be burdensome and could result in incomplete eradication of the infection following non-compliance and ultimately development of resistance[13]. Moreover, currently prescribed treatment options present with adverse side effects such as dyspepsia and altered bowel habits and could further discourage patients from completing the prescribed course, a concern that has been linked to the development of resistant *H. pylori* strains.

Put together, these pressing challenges have necessitated the search for safer and more effective alternatives for treatment of ulcers caused by *H. pylori* from diverse sources that include natural bioactive compounds from plants[14,15]. One of such plants with promising bioactive compounds is *Aloe vera*, which contains diverse bioactive compounds, including flavonoids, lectins, terpenoids, anthraquinones, fatty acids, salicylic acid, mono- and polysaccharides, enzymes, vitamins, and minerals[16–19]. *A. vera* is well recognised for its broad spectrum of medicinal properties, including anti-inflammatory, antimicrobial, antioxidant, anti-cancer, cardioprotective, anti-diabetic, prebiotic, bone-protective, and skin-healing effects[20]. Notably, several in vitro and assay-based studies have reported the inhibitory activity of *A. vera*-derived compounds against *H. pylori*, supporting its potential as a natural anti-*H. pylori* agent[21–23].

From its pool of bioactive compounds, we selected esculetin, aloe emodin, chrysophanic acid, and aloesin for an in silico study against the NAP of *H. pylori*. Docking and molecular dynamic (MD) simulations are essential for evaluating their binding potential and stability within the NAP active site. Esculetin, a coumarin derivative, has hydroxyl groups at the 6 and 7 carbon positions, enabling strong hydrogen bondings with key residues in NAP. Aloe emodin and chrysophanic acid, both anthraquinones, contain hydroxyl and carbonyl groups that facilitate hydrogen bonding, electrostatic interactions, and π-π stacking, potentially stabilising their binding to NAP. Aloesin, a glycosylated chromone, has multiple hydroxyl groups, increasing its solubility and ability to form hydrogen bonds which may interfere with the protein's function. These diverse compounds will allow for the evaluation of the effect of diverse functional groups that could enhance their ability to interact with the target protein (NAP) and potentially disrupt its pro-inflammatory activity. Our choice of the NAP is due to its already established role in promoting inflammation and oxidative stress, which contribute to ulcer formation. Targeting NAP with these bioactive compounds offers a promising therapeutic approach due to their anti-inflammatory, antioxidant, and antimicrobial properties. Thus, our study aims to evaluate the anti-*H. pylori* of the aforementioned compounds using docking and molecular dynamics (MD) simulations.

Methods

Ligands and protein retrieval

In this study, we utilised bioactive compounds previously reported in the literature[19]. The selected compounds were aloe-emodin (PubChem CID: 10207), chryosophanic acid (PubChem CID: 10208), esculetin (PubChem CID: 5281416), and aloesin (PubChem CID: 160190). The compounds were selected based on reported experimentally validated biological activities that including antimicrobial, anti-inflammatory, anti-cancer, cardioprotective, anti-diabetic effects, and antioxidant properties[20]. Furthermore, we selected the compounds to evaluate the interactions of their diverse functional groups, particularly hydroxyl and carbonyl moieties on the target protein. On the other hand, from the Research Collaboratory for Structural Bioinformatics (RCSB) database, we selected the *H. pylori* Neutrophil-Activating Protein (NAP) (PDB ID: 1JI4)[24]. The NAP is a key virulence protein that initiates a cascade of events contributing to ulcer pathogenesis[4,5,24].

Ligands and target protein preparations

The structures of the ligands were first sketched using ChemDraw Ultra version 9.0[25], and their energies were minimised using the MMFF94 force field. Following energy minimisation, the ligands were stored for further use. The SMILES strings of the ligands were also retrieved for the prediction of ADMET properties. The target protein, neutrophil-activating protein (NAP) from *H. pylori* (PDB ID: 1JI4), was prepared using BIOVIA Discovery Studio[26]. After loading the protein to reveal the native ligand, the structure was first inspected for missing residues or atoms and no significant gaps were identified. Next, all the water molecules and heteroatoms, including co-crystallised ligands and ions, were removed to prevent interference with docking calculations. Hydrogen atoms were added to the protein structure to maximise the protonation state at physiological pH (7.4),

and partial charges were also removed. Using the CHARMm force field, the protein was subsequently subjected to energy minimisation with minimisation steps set to 1000 iterations and a convergence gradient of 0.01 kcal/mol/Å² to relieve steric clashes and optimise geometry. The resulting structure was saved in PDB format and used for subsequent docking studies[27].

Molecular docking

To assess ligand binding affinities and identify key interacting amino acid residues, molecular docking was carried out. Molecular docking has emerged as powerful tool in the search for safer and more effective ligands with therapeutic properties[28–31]. Docking was performed as described in a previous study[32]. The protein's allosteric pocket was identified using the Site Finder tool in molecular operating enviroment (MOE). The coordinates of the active site were determined to be X = 24.5016, Y = 14.8366, and Z = 1.0583. To ensure reproducibility, we performed docking using the Autodock Vina tool version 1.2.0[33]. In the tool, the prepared ligands were individually docked to the target protein. The London dG scoring algorithm which has been validated in various studies was utilised to compute the binding scores[26]. Following docking, the best poses were visualised in 2D using BIOVIA Discovery Studio[26].

Molecular dynamics simulations

To assess the stability of the complexes, a 300-nanosecond molecular simulation run was carried out using the Schrodinger Desmond module and the Optimised Potentials for Liquid Simulations (OPLS) force field. The system was solvated using the TIP3P water mode, while the simulation box was orthorhombic with a boundary of 10 Å. The solvated system was neutralised by adding appropriate counter ions, and the osmotic state was maintained by the addition of 0.15 M NaCl. The system was equilibrated prior to the simulation run. The simulation run was carried out at a pressure and temperature of 1.013 bar and 310 K[27,28].

Density functional theory (DFT) study of the ligands

Ligand reactivity was evaluated through Density Functional Theory (DFT) calculations, a quantum mechanical method that enables the prediction of molecular reactivity and electronic properties[34]. The analysis was conducted using the Gaussian 09 program. Geometry optimisations and energy calculations were initially conducted using the B3LYP functional with the 6-31G(d, p) basis set, which is suitable for organic molecules comprising carbon, hydrogen, nitrogen, and oxygen atoms. To enhance the accuracy of the electronic descriptors and better account for polarisation and diffuse effects, further optimisations were carried out using the B3LYP/6–31 + G(d, p) level of theory[27,28]. These computations provided insights into the frontier molecular orbitals, energy gaps, and overall electronic reactivity of the selected ligands[27,28].

Prediction of ADMET properties and evaluation of the lipinski's ROF of the ligands

The pkCSM tool was used to predict ADMET properties and their molecular descriptors. After prediction, the molecular descriptors were assessed for compliance with the Lipinski's rule of five[35–37].

Results and discussions

Molecular docking and simulation dynamics of the formed complexes

We explored the anti-*Helicobacter pylori* potential of selected *A. vera* bioactive compounds using in silico approaches. Table 1 presents the molecular docking results of the ligands against the neutrophil-activating protein (NAP) of *H. pylori* (PDB ID: 1JI4). The docking scores varied across the test ligands, all of which exhibited stronger binding affinities than the control native ligand, which returned the lowest binding affinities of − 4.3 kcal/mol. The test ligands showed more favourable binding energies, ranging from − 6.3 to − 7.4 kcal/mol. Specifically, esculetin, aloe-emodin, and chrysophanic acid recorded binding affinities of − 6.3, − 6.4, and − 6.4 kcal/mol, respectively, while aloesin demonstrated the strongest binding with a docking score of − 7.4 kcal/mol. These higher negative binding affinities observed for the test ligands, compared to the native ligand, suggest a higher binding affinity and stronger potential for inhibitory activity against the NAP protein. This finding aligns with previous reports indicating that, in molecular docking studies, more negative binding energies are associated with more favourable interactions and stronger ligand–protein binding affinities[38]. The binding affinities observed in our study are consistent with a previous report that evaluated the in silico properties of *A. vera* phytoconstituents[21]. In that study, seventeen compounds, including aloesin, aloe-emodin, and chrysophanic acid, were docked against glucosamine-6-phosphate synthase, a key enzyme involved in bacterial cell wall synthesis. The results demonstrated notable binding affinities ranging from 0 to − 12.419 kcal/mol, indicating potential antibacterial activities. In another study, docking scores that ranged from − 6.4 to −9.73 kcal/mol were observed for the various natural inhibitors[39]. The variation in docking scores between the two studies may be attributed to the use of different target proteins. While our study focused on the neutrophil-activating protein (NAP) of *H. pylori*, their studies investigated glucosamine-6-phosphate synthase and outer membrane protein 6 (OMP6). Notably, aloe-emodin was shown to inhibit *H. pylori* biofilm formation by targeting OMP6[22]. The antibacterial potential of *A. vera* phytoconstituents has also been supported by other studies combining both in vitro and in silico approaches[21,22].

Table 1 presents the results of the interacting residues, bond types, and bond distances for each of the ligands and the control. The control exhibited the weakest binding energy, ranging from − 0.1 to − 1.9 kcal/mol, with bond distances between 2.56 and 2.90 Å, primarily forming hydrogen bonds (acceptor and donor) with residues Glu46, Tyr99, and Ser135. In contrast, the test ligands demonstrated stronger binding interactions, consistent with the higher binding affinities observed. Binding energies ranged from − 0.8 to − 1.3 kcal/mol for aloe-emodin, − 0.4 to − 6.9 kcal/mol for aloesin, and − 0.8 to − 2.3 kcal/mol for esculetin. The specific interacting

Ligand	Receptor	Interaction	Distance	E (kcal/mol)	Binding affinties (kcal/mol)
1ji4/control					−4.3
O4 17	OE1 GLU 46	H-donor	2.56	−0.1	
O2 10	OH TYR 99	H-acceptor	2.90	−1.9	
O2 10	OG SER 135	H-acceptor	2.89	−1.4	
1ji4/10,207 (Aloe emodin)					−6.4
O5 25	OE1 GLN 128	H-donor	2.75	−1.3	
O2 1	CA ILE 43	H-acceptor	3.38	−0.8	
1ji4/10,208 (Chrysophanic acid)					−6.4
O3 2	OG SER 135	H-acceptor	2.75	−2.0	
1ji4/160,190 (Aloesin)					−7.4
O8 2	SD MET 138	H-donor	3.75	−0.4	
O6 32	OE1 GLN 128	H-donor	2.59	−2.3	
O3 36	O ILE 43	H-donor	2.71	−2.6	
O8 2	NZ LYS 134	H-acceptor	2.77	−6.9	
O9 46	OG SER 135	H-acceptor	2.66	−1.9	
1ji4/5,281,416 (Esculetin)					−6.3
O2 16	OE1 GLN 128	H-donor	2.65	−1.4	
O3 18	SD MET 50	H-donor	3.66	−2.3	
O4 2	OH TYR 99	H-acceptor	3.07	−0.8	
O4 2	OG SER 135	H-acceptor	2.73	−1.4	

Table 1. Docking properties of the complexes formed.

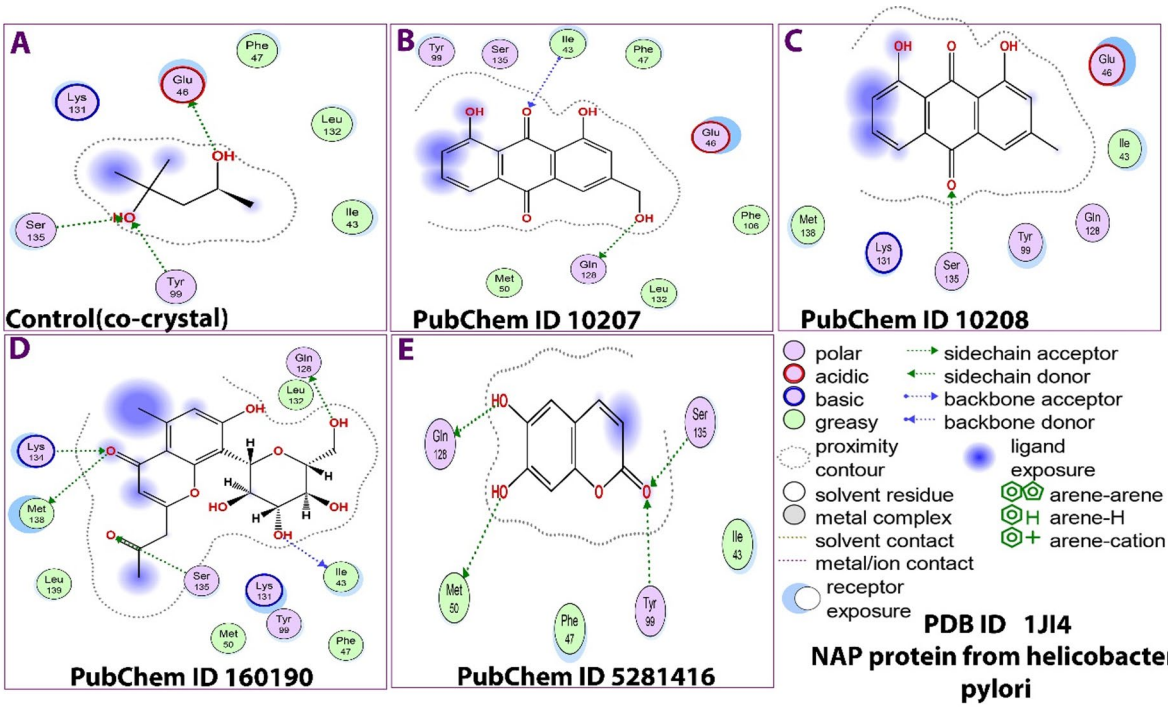

Fig. 1. A 2D representation of the docking poses of the various test ligands and control with the target protein (PDB iJI4 NAP protein from *H. pylori*).

residues varied across the ligands: aloesin (PubChem CID: 160190) formed interactions with five residues (Met138, Gln128, Ile43, Lys134, and Ser135), the highest among all, while esculetin (CID: 5281416) interacted with four residues (Gln128, Met50, Tyr99, and Ser135). These findings support the binding affinities reported in Table 1 and reveal that Ser135 was involved in all ligand interactions, suggesting its potential significance in mediating the inhibitory effects of the selected *A.vera* phytoconstituents.

In addition to Table 1; Fig. 1 shows the result of the docking (poses) in 2D for the control and test ligands. The results indicate the presence of basic, acidic, polar, and greasy interactions among the ligands and amino acid

residues. Furthermore, in all the poses, ligand exposure was observed and various amino acids involved in the bonding revealed. The various bonds were acid, polar and basic, with polar and basic bonds being the dominant ones. All compounds fitted inside the binding pockets and interacted with different amino acids in terms of numbers and type. Furthermore, various amino acid residues were within the proximity contours and these were 11, 6, 7, 9, and 7 for ligands 160190, 5281416, 10208, 10207, and control. The amino acids were same as those captured in Table 1 and these were Phe47, Glu46, Lys131, Ser135, Tyr99, Leu132 and Ile43 for the control. For ligand 10207, in addition to those found in the control, Phe106, Met50, and Gln128 were also involved in the docking. For ligand 10208, the residues were Glu46, Ile43, Gln1288, Tyr99, Ser135, Lys131 and Met138. For ligand 169190, the amino acids were similar to those of the control but in addition, it had Met138, Leu139, Leu139 and Glu128. For ligand 5,281,416, the amino acids were Ser135, Ile43, Tyr99, Phe47, Met50, and Glu128.

The docking results of the various test native (control) ligands against the *H. pylori* neutrophil-activating protein (NAP; PDB ID: iJI4) revealed that all compounds were successfully accommodated within the protein's binding pocket. The NAP is a major virulence factor of *H. pylori* that contributes to its pathogenesis by stimulating neutrophils, promoting inflammation, and aiding immune evasion[4,5]. The control ligand interacted with residues, including Phe47, Glu46, Lys131, Ser135, Tyr99, Leu132, and Ile43, amino acids crucial for structural stability and protein-protein interactions. Residues like Glu46 and Lys131 are capable of forming electrostatic interactions that stabilise the protein's oligomeric form, while Ser135 and Tyr99 likely to mediate hydrogen bonding. Ligand 10207 interacted with additional residues, including Phe106, Met50, and Gln128, suggesting a broader binding interface that may enhance stability or binding affinity[23]. Ligand 10208 also bound to Met138, a residue close to the C-terminal that may influence oligomerisation. Furthermore, ligand 160,190 exhibited interactions similar to the control but also included Glu128, Met138, and Leu139, which may likely disrupt subunit assembly or iron coordination[23]. Ligand 5281416 interacted with both polar and hydrophobic residues such as Ser135, Glu128, and Met50, suggesting potential to modulate NAP's structural dynamics. Overall, residues Glu46, Lys131, Phe47, Ile43, and Leu139 are central to the stability and function of NAP. Their interaction with the ligands suggests a mechanism of inhibition that may impair *H. pylori*'s neutrophil-activating ability, reducing its virulence. In addition, the number of amino acid residues involved in the various interactions appeared to align with the docking scores of the ligands utilised in this study. The highest number of amino acid residues was observed for ligand 160,190, further indicating the role of amino acids in the docking process and preferential interactions[37].

Docking alone cannot provide any insight into the stability of a protein as it complexes with various ligands[28,40]. To evaluate the stability of the protein in the presence of the ligands as well as the conformational dynamics of the protein-ligand complexes post-docking, a 300 ns molecular dynamics (MD) simulation was carried out. Root Mean Square Deviation (RMSD) is a quantitative measure of the structural deviation between atomic positions in a molecular system over time[41]. RMSD is one of the critical parameters that is deployed to analyse a protein–ligand complex, especially its backbone C-α atoms. It is alsoused to indicate a protein's overall conformational stability in a dynamic state as obtained during simulation. Figure 2 presents the Root Mean Square Deviation (RMSD) profiles over a 300 ns molecular dynamics simulation. The RMSD values exhibited some variation across the complexes for the duration of the simulation. The control returned RMSD values that ranged from 1.0 to 2.8 Å. Ligand 10,207 gave protein RMSD values between 0.9 and 2.6 Å, and ligand RMSD values ranging from 6.0 to 54.0 Å. For ligand 10,208, the RMSD values ranged from 1.2 to 2.6 Å for the protein and 1.5 to 12.0 Å for the ligand. In the case of ligand 160,190, protein RMSD values ranged from 1.2 to 2.8 Å, while ligand RMSD values extended from 0.0 to 56.0 Å. The most stable complex was that formed between the protein and ligand 5,281,416 which showed stable RMSD values that were well within the acceptable 3Å throughout the duration of the simulation[27,40]. Ligand 10208, experienced some fluctuations at the start and around 130 ns but it later stabilised. Ligand 160,190 also shows stable conformation at the start of the run but experienced fluctuations between 210 and 230 ns, and later stabilised thereafter. The rest of the ligands especially the control was unstable for the most part of the simulation run. Our findings indicate that the control protein RMSD values ranged from 0.9 to 2.8 Å. This low and almost similar protein RMSD values across complexes suggest that the protein maintains structural integrity upon binding with the various ligands. Generally, RMSD values less than 4 Å are generally regarded as stable[27,40]. Furthermore, the stability observed across all ligand-bound complexes suggests that the ligands closely resemble the control in behaviour and do not induce significant conformational changes in the protein. The consistently low RMSD values indicate that the docking poses were retained throughout the simulation and that the ligands remained well accommodated within the binding site. This structural stability reinforces the docking results, suggesting that the predicted binding modes were reliable. Notably, ligands 5281416 and 10208, which showed favourable docking scores and higher numbers of interacting residues, also exhibited stable RMSD trajectories, further supporting the validity of their binding conformations. Overall, the protein RMSD trajectories for all ligand-bound complexes were comparable to that of the control, suggesting that the protein maintained structural stability throughout the simulation regardless of the ligand bound.

In addition, the agreement between docking and RMSD findings enhances confidence in the predicted binding affinities and supports the hypothesis that these ligands form stable complexes with the NAP protein.

Figure 3 shows the results of the RMSF values of the formed NAP-ligand complexes. The result as expected showed variations. For the control, the values ranged from 0.5 to 3.0 Å but there were spikes above 2 Å at amino acid residues at positions 30, 80 and 140. For ligand 10207, the RMSF values ranged from 0.4 to 2.0 Å, however, there also spikes with RMSF above 1.6 Å at residues 30, 80 and 140. For ligand 10,208, the RMSF value ranged from 0.4 to 2.2 Å with spikes above 2 Å at residues 80 and 140, respectively. For ligands 160,190 and 5,281,416, the RMSF ranged from 0.5 to 2.4 Å and 0.5 to 4.0 Å, but there were spikes above 2 Å around amino acid residues at positions 30, 85 and 140, respectively. As a parameter like RMSD, low and consistent values indicate stability while higher RMSF values indicate low stability and also major changes in a bid to obtain a stable state[42]. Also, regions of elevated RMSF indicate regions of increased flexibility, which may influence

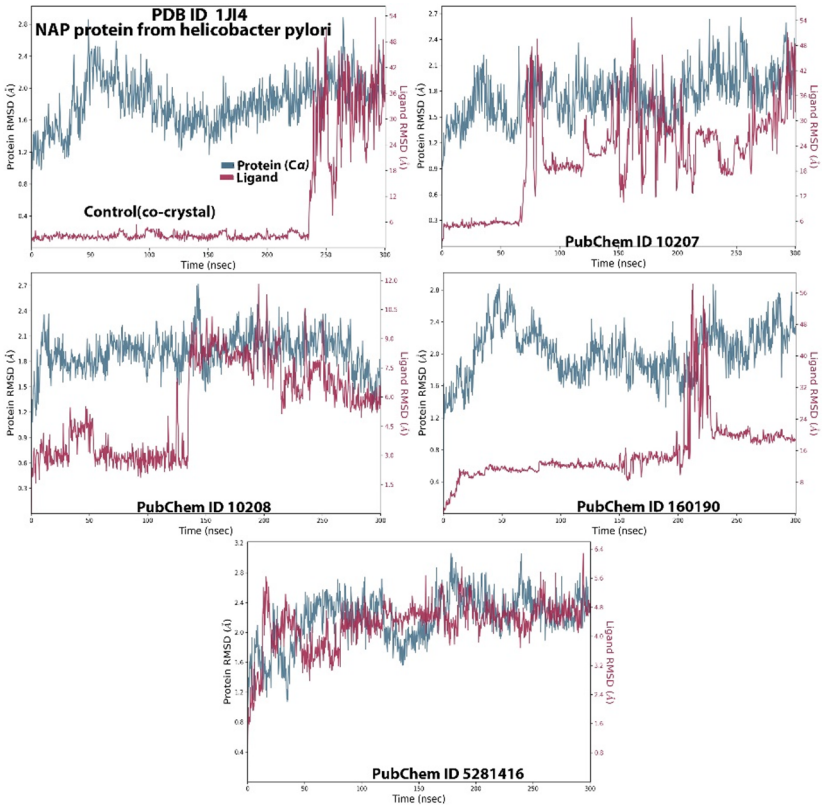

Fig. 2. RMSD plots of the various ligands and target protein.

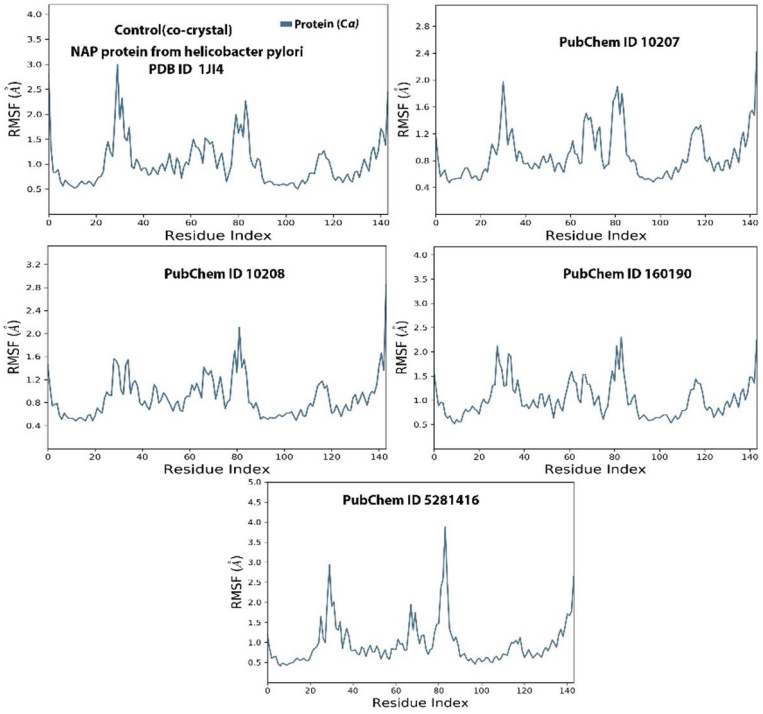

Fig. 3. RMSF plots of the various complexes and their test ligands.

ligand binding and overall protein stability[28]. In our study, it was noted that at amino acid residues 30, 80/85, and 140, consistently higher fluctuations occurred across the different complexes, indicating their potential role in dynamic interactions. Specifically, these residues correspond to regions of structural and functional activities in the NAP target protein.

Residue 30 lies within a surface-exposed loop, suggesting that the flexibility of the region may accommodate conformational adjustments upon ligand binding interactions. Residues 80/85 are situated close to the ferroxidase channel and may play roles in ligand access, metal coordination, or stabilising the catalytic pocket. Meanwhile, residue 140 lies near the C-terminal helix, a region noted for its dynamic nature and possible involvement in oligomer stability and allosteric regulation[43]. Together, the observed consistency between docking affinities, interaction profiles or the residues involved, and observed stable simulation values (RMSD, RMSF) strengthens the validity of the docking results and confirms the dynamic compatibility of the selected ligands with the target protein and its flexibility of the target as it binds with the study ligands.

The ranking of the ligands using their docking scores and RMSD values as presented in Table 2 indicates that chrysophanic acid and esculetin ranked first and second. Aloesin recorded the strongest binding affinity (−7.4 kcal/mol), indicating strong binding affinity, but showed the least structural stability, with RMSD rising above 16 Å for a significant duration. Aloe emodin, despite a good docking score (−6.4 kcal/mol), also showed poor stability after 70 ns, reaching up to 54 Å. In contrast, chrysophanic acid maintained a consistently low RMSD profile, staying below 10 Å throughout and ranking highest in stability. Esculetin demonstrated both favourable binding and structural integrity, with RMSD ranging between 1.5 and 11 Å. The control compound was initially stable but showed a steep increase in RMSD beyond 230 ns.

Figure 4 shows the results of the interactions, the different bond types and the respective amino acids involved in the various bonds. The results indicate that hydrogen, hydrophobic, ionic and water bridges were the main bond types. Water bridges were the most dominant bond followed by hydrogen bond. The number of amino acids involved in the interacting fractions returned a total of 43, 92, 19, 51, and 15, respectively.

Figure 5 presents the results of the contact analysis performed during the simulation. The findings show that both the control and test ligands formed multiple contacts with the target protein throughout the simulation run. The total number of contacts recorded were 6, 12, 6, 9, and 6 for the control and ligands 10207, 10208, 160190, and 5281416, respectively. Notably, ligands 5281416 and 10208 engaged a greater number of amino acid residues, suggesting more extensive interactions. For ligand 10,208, the key interacting residues were Glu42, Glu46, Tyr99, and Ser135. Ligand 5,281,416 interacted primarily with Glu46, Asp53, and Tyr99. In the case of ligand 160190, Glu42 and Met138 were the residues with the most persistent or strongest contacts. The control ligand formed interactions with Glu46, Phe47, Tyr99, Gln128, and Lys131. These findings highlight differences in contact profiles across the ligands, potentially reflecting variations in binding strength and stability. Our analysis of interaction fractions within the protein–ligand complexes revealed that hydrogen bonds and water bridges were the predominant types of non-covalent interactions, with water bridges occurring the most. These findings are consistent with previous studies highlighting the crucial role of hydrogen bonding and solvent-mediated interactions in complex stabilisation[27,39,42,44–46]. Water bridges, in particular, suggest active participation of surrounding water molecules in mediating and stabilising ligand binding, which may contribute to dynamic stability within the binding pocket[43]. The predominance of these interactions correlates with the observed binding affinity trends from molecular docking. Complexes with higher interaction fractions, especially involving hydrogen bonds and water bridges, also demonstrated more favourable binding energies, suggesting a functional link between these stabilising forces and binding strength. Furthermore, our contact analysis showed that ligands 5,281,416 and 10,208 formed more extensive contacts with the protein, with residues Glu42, Glu46, Tyr99, and Ser135 involved. These residues are functionally significant and contribute to protein structural integrity and specificity.

In particular, the residues Glu42, Glu46, Tyr99, and Ser135 were all within or near the active site of the target protein as revealed by the molecular docking, suggesting their functional relevance. The presence of glutamic acid residues (Glu42 and Glu46)often involved in the catalytic activity and electrostatic interactions of the target, suggest a role for substrate identification and enzymatic function[48]. As an amino acid, glutamic acid (Glu) residues can form ionic and hydrogen bonds, contributing to structural integrity and interaction specificity[44]. In addition, the presence of Tyr99, also located in the within the binding pocket of the target protein, can participate in the formations of π–π stacking, hydrophobic and hydrogen bonds, thereby influencing ligand positioning and binding affinity[49]. In the same vein, Ser135 possess a hydroxyl group that is capable of forming hydrogen bonds and it is routinely implicated in substrate recognition and interaction specificity[50]. Overall, the involvement of these residues implies that they may be critical in the modulation of protein function, either by hindering substrate access or by initiating conformational changes atypically related with allosteric modulation.

Rank	Ligand	Docking scores (kcal/mol)	Summary of RMSD	Overall stability assessment
1	Chrysophanic acid	−6.4	< 5 Å for 0–130 ns; 6–10 Å for remainder	Most stable overall, limited deviation
2	Esculetin	−6.3	1.5–4.5 Å for 0–130 ns; 5–11 Å thereafter	Very stable early on; moderate rise later
3	Control ligand	−4.3	< 3 Å for 0–230 ns; then rises sharply to 6–54 Å	Stable for long, then large instability
4	Aloe emodin	−6.4	< 5 Å for 0–70 ns; then 12–54 Å	Short early stability; large deviation
5	Aloesin	−7.4	< 16 Å for 0–220 ns; then 16–24 Å	Highest RMSD overall; significant fluctuations

Table 2. Ranking of the ligands based on their Docking scores and RMSD values.

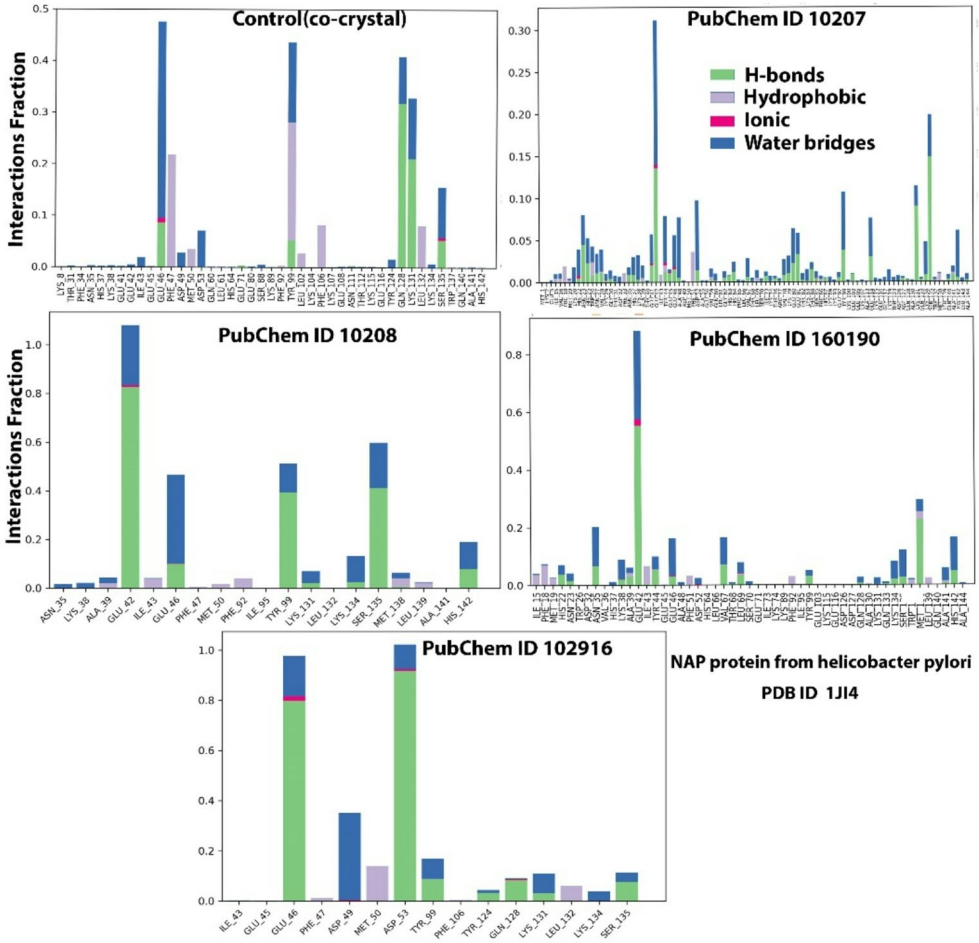

Fig. 4. Interacting fractions, various interactions and their respective amino acids.

Ligand properties

To further provide insight into the stability and flexibility, compactness, as well as the ligand's surface characteristics and potential interaction sites, we further explored the RMSD, rGyr, MolSA, SASA, and PSA properties of the ligands[27,40,42]. Collectively, these parameters provide comprehensive insights into the conformational stability and dynamic behaviour of the ligands within their respective complexes. The results of the ligand property analysis are presented in Fig. 6. The RMSD values ranged from 0 to 1.4, 0.25 to 0.75, 0.6 to 1.2, 0.5 to 3, and 0.2 to 1.2 Å for the control and ligands 10207, 10208, 160,90, and 5281416, respectively.

For the rGyr, the values were 1.92 to 2.16, 3.1 to 3.4, 2.94 to 3.12, and 3.6 to 4.05, and 2.45 to 2.60, respectively. The MolSA values were 140 to 148, 250 to 260, 246 to 255, 340 to 370, and 154.5 to 159, respectively, for control and ligands 10207, 10208, 160190, and 5281416. The PSA values were 60 to 90, 165 to 195, 120 to 165, 225 to 300, and 165 to 175, respectively, for control and ligands 10,207, 10,208, 160,190, and 5,281,416. Overall, the low RMSD values indicate that the ligands were stable, even better than the control, except for ligand 160,190, which returned slightly higher RMSD values than the control, and this aligns with previous reports[28,41]. The observed stability is crucial for the effective binding of the ligands and suggests consistent ligand-ligand positioning can enhance binding affinity and specificity. The rGyr values indicate that the ligands were generally compact, with 528,416 returning the most compact value among the ligands with its lowest rGyr value[48]. A more compact structure has the potential to influence the ligand's ability to fit tightly into the binding pocket of the protein and indicates stability together with RMSD values[48].

Together with MolSA, the PSA values provide insights into the ligand's surface characteristics and potential interaction sites[28,41,44]. The MolSA values ranged from 140 to 370 Å², SASA from 60 to 300 Å², and PSA from 60 to 300 Å² across the control and ligands. The large values for MolSA, the PSA observed for ligand 160190 suggest increased exposure to solvent, which can affect the ligand's solubility and interaction dynamics. A higher PSA indicates a greater polar region, potentially enhancing hydrogen bonding with the target protein, and this corroborates the higher docking score and hydrogen bonds observed for ligand 160,190[50].

We further conducted the Principal Component Analysis (PCA) to determine the dominant motions within the molecular dynamics simulations[41]. The result of the PCA analysis is presented in Fig. 7. The results indicate that PC1, PC2, and PC3 for each of the ligands varied for the control and test ligands. For ligand 10207, the respective PC values were 19.6, 10.0, and 6.65, respectively, while for ligand 10208, the values were 18.47, 12.18,

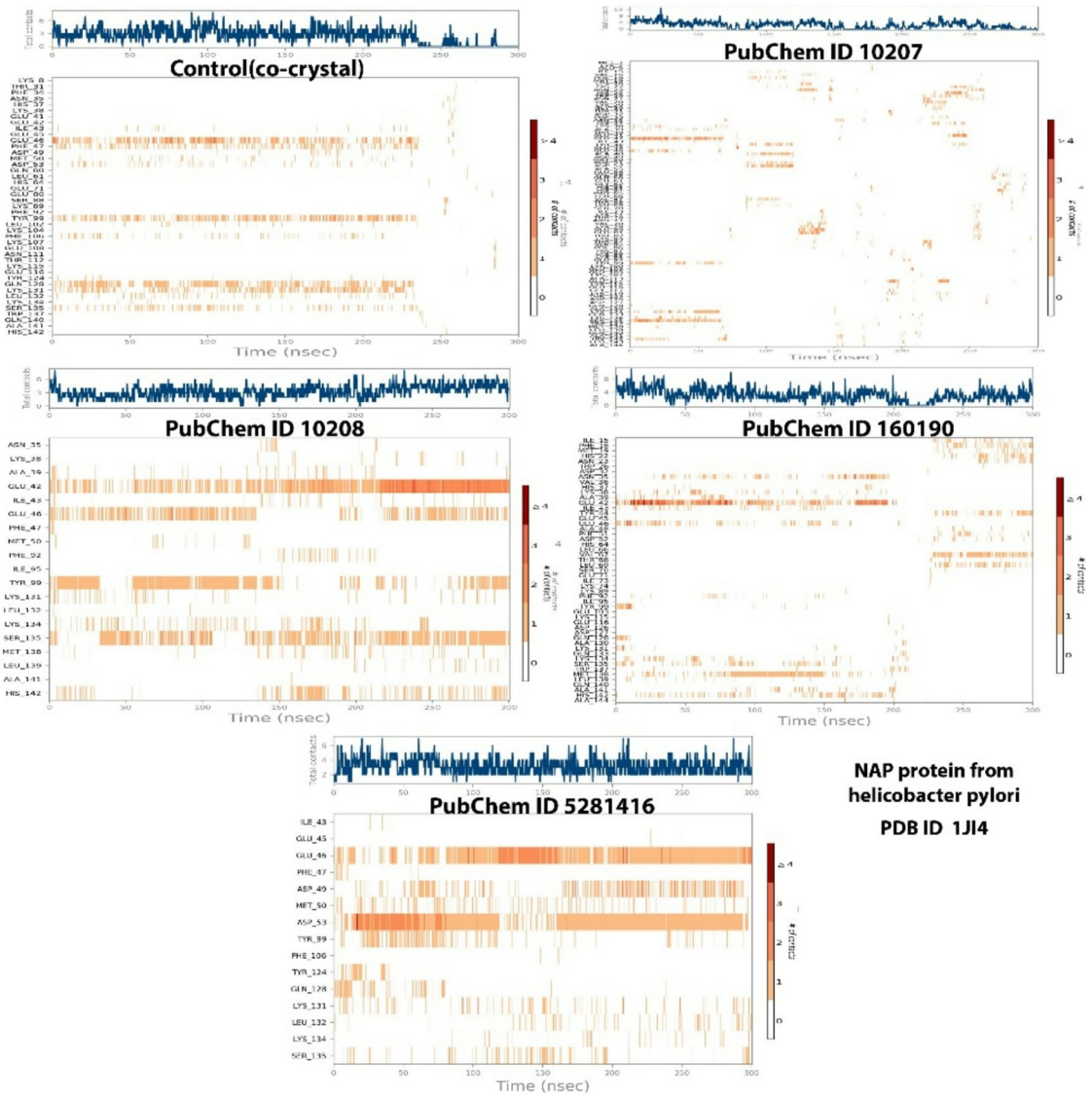

Fig. 5. Contact analysis plot of the various complexes at 300 ns.

and 9.88, respectively, for PC1, 2, and 3. For ligand 16190, the PC values were 21.69, 18.47, and 6.83, while for 5281416, the values were 31.06, 15.63, and 9.67, respectively, for PC1, 2, and 3. For the control, the values were 19.4, 14.59, and 4.59, respectively, for PC1, 2, and 3. The values varied as expected and in line with a previous report[40]. Ligand 5281416 exhibited the highest PC1 value at 31.06, suggesting significant conformational flexibility. In contrast, ligands 10207 and 10208 showed lower PC1 values (19.6 and 18.47, respectively), indicating more restricted movements. Put together, the PCA findings align with the RMSD and rGyr results and overall indicate the stable complexes.

ADMET properties

Tables 3 and 4 show the results of the predicted ADMET and molecular descriptors for the ligands.The ADMET and molecular descriptor analysis provided further insights into the pharmacokinetics and drug-likeness of esculetin, aloe emodin, chrysophanic acid, and aloesin. The water solubility values of the studied bioactive compounds were − 2.497, −3.104, −3.077, and − 2.309, respectively, for esculetin, aloe emodin, chrysophanic acid, and aloesin. The $CaCO_2$ permeability for the ligands were 0.301, −0.233, 1.298 and 0.305, respectively for esculetin, aloe emodin, chrysophanic acid, and aloesin. Intestinal absorption in humans for the various ligands ranged from 46.247 to 96.558, while that of the control was 85.07, which was within the range of the studied ligands. Skin permeability for the ligands ranged from − 0.233 to 1.298, while the intestinal absorption for the ligands ranged from 46.25 (aleosin) to 86.29 (esculetin). All ligands were substrates for P-glycoprotein except the control, while all the ligands, as well as the control, were not inhibitors of P-glycoprotein I and II. The predicted VDss (human) values ranged from 0.212 to 0.671 for the ligands, while that of the fraction unbound, BBB, and CNS ranged from 0.226 to 0.484, −0.792 to 0.212, and − 3.783 to −2.296, respectively, for esculetin, aloe emodin,

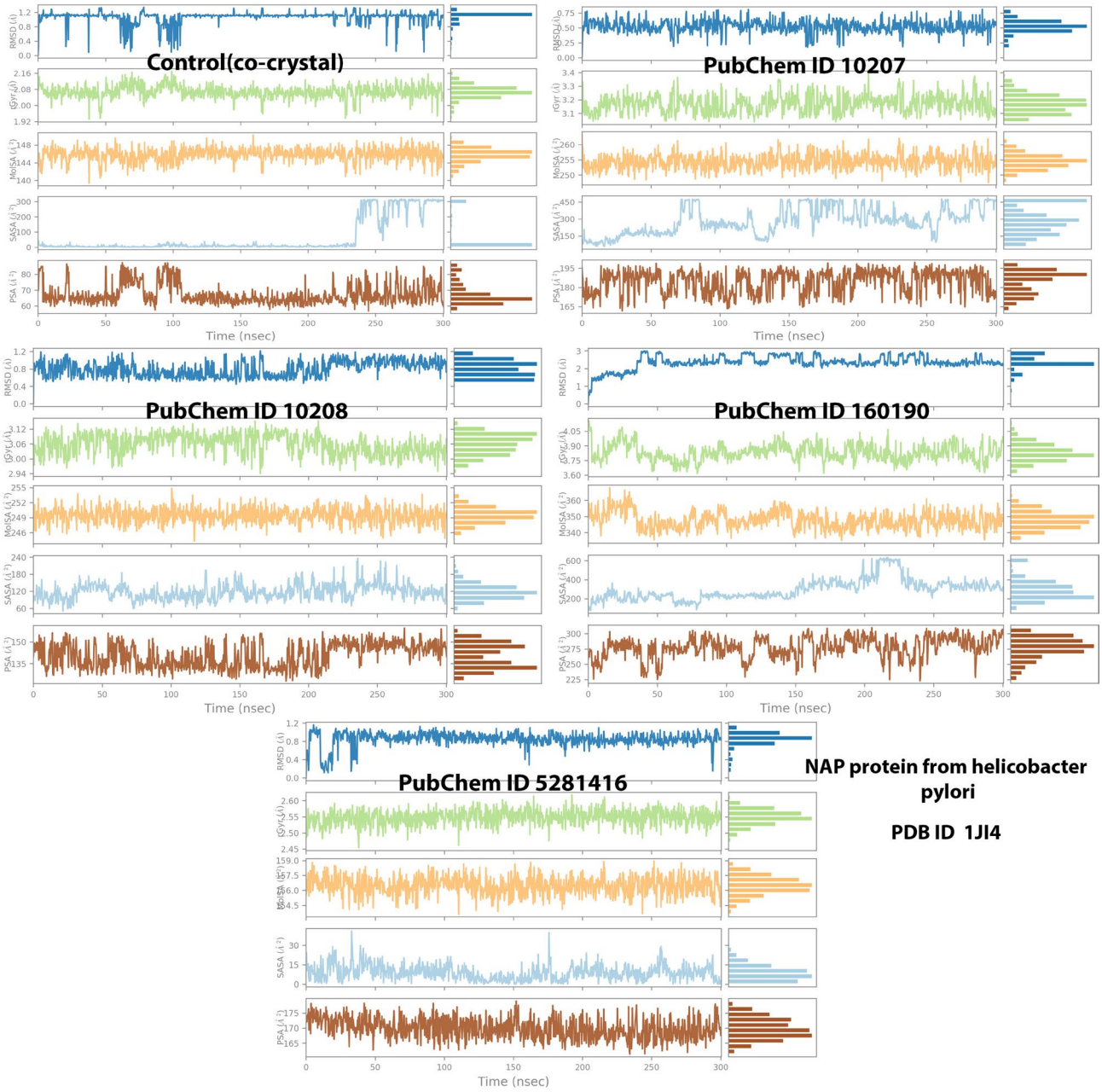

Fig. 6. The RMSD, rGyr, MolSA, SASA, and PSA evaluations of the ligands at 300 ns.

chrysophanic acid, and aloesin. Overall, the compounds exhibited moderate solubility (−2.497 to −3.104)[50], variable $CaCO_2$ permeability (0.301 to −0.233), and intestinal absorption (46.25% to 96.56%), with esculetin showing the highest absorption[52]. Limited blood-brain barrier permeability (−0.792 to 0.212) suggests minimal CNS effects[53].

Gaining an understanding of the metabolic state of ligands is important for providing insight into their pharmacokinetic behaviour and potential for drug–drug interactions[54,55]. In this study, we evaluated the metabolism of esculetin, aloe emodin, chrysophanic acid, and aloesin, focusing on their inhibitory and substrate potential across the breast cancer resistance protein (BCRP), cytochrome P450 enzymes (CYPs), and drug transporters. The interactions of ligands either as substrates or inhibitors have pharmacokinetic implications[54].

Among all the cytochrome P450 enzymes, the isoforms CYP1A2, CYP2C19, and CYP2D6 were the most affected. Among the ligands, aloe emodin and chrysophanic acid were predicted to inhibit multiple CYP isoforms with high confidence, showing strong inhibitory potential for CYP1A2 and CYP2D6, and moderate to high confidence for inhibition of CYP2C19. These CYP enzymes are involved in the metabolism of a wide range of clinically important drugs, and their inhibition by potential therapeutic compounds, as observed with our ligands, may result in elevated plasma concentrations of such medications[56]. Chrysophanic acid was also predicted to be a substrate for CYP1A2, CYP2C19, and CYP2C9, indicating that the compound is likely to

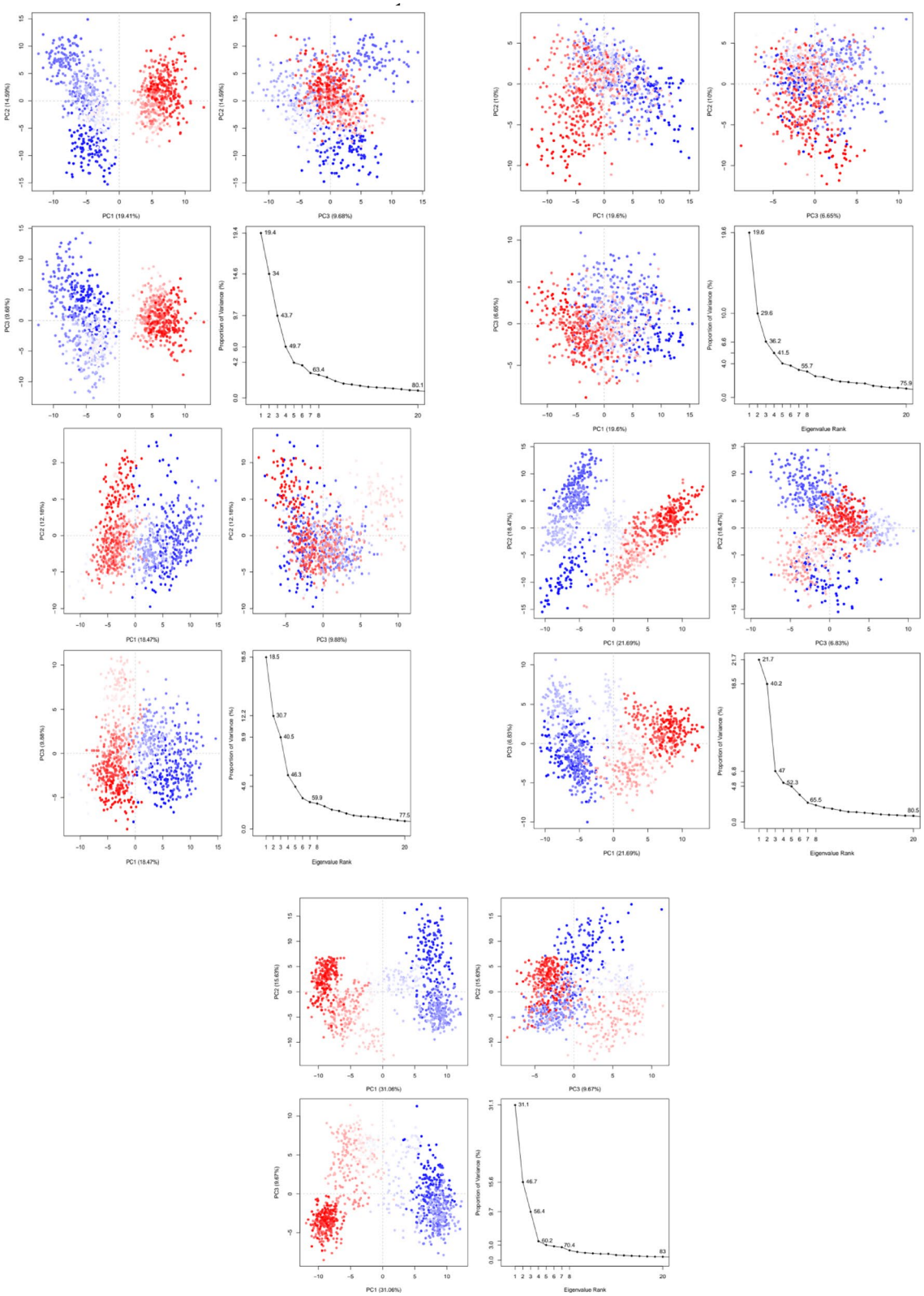

Fig. 7. Principal component analysis (PCA) of the various complexes.

undergo hepatic biotransformation, which could affect its bioavailability and rate of elimination[56]. On the other hand, esculetin and aloesin were predicted to have the lowest interaction profiles. Specifically, both compounds were identified as non-inhibitors of major CYP enzymes, including CYP3A4, CYP2D6, and CYP2C19, with medium to high confidence. This suggests a lower risk of metabolic drug–drug interactions. However,

ADMET	Esculetin	Aloe emodin	Chrysophanic acid	Aloesin
Absorption				
Water solubility	−2.497	−3.104	−3.077	−2.309
$CaCO_2$ permeability	0.301	−0.233	1.298	0.305
Intestinal absorption (human)	86.291	74.179	96.558	46.247
Skin permeability	−2.796	−2.743	−2.83	−2.736
P-glycoprotein substrate	Yes	Yes	Yes	Yes
P-glycoprotein I inhibitor	No	No	No	No
P-glycoprotein II inhibitor	No	No	No	No
Distribution				
VDss (human)	0.528	0.671	0.272	0.212
Fraction unbound (human)	0.484	0.226	0.154	0.416
BBB permeability	0.025	−0.729	0.212	−1.29
CNS permeability	−2.296	−2.466	−2.111	−3.783
Metabolism				
CYP2D6 substrate	No	No	No	No
CYP3A4 substrate	No	No	No	No
CYP1A2 inhibitor	Yes	Yes	Yes	No
CYP2C19 inhibitor	No	No	No	No
CYP2C9 inhibitor	No	No	No	No
CYP2D6 inhibitor	No	No	No	No
CYP3A4 inhibitor	No	No	No	No
Excretion				
Total clearance	0.671	0.008	0.02	0.456
Renal OCT2 substrate	No	No	No	No
Toxicity				
AMES toxicity	No	Yes	Yes	No
Max. tolerated dose (human)	−0.262	−0.089	−0.256	0.437
hERG I inhibitor	No	No	No	No
hERG II inhibitor	No	No	No	No
Oral rat acute toxicity (LD50)	2.337	2.329	2.275	2.47
Oral rat chronic toxicity (LOAEL)	1.504	1.878	2.057	3.95
Hepatotoxicity	No	No	No	Yes
Skin sensitisation	No	No	No	No
T.Pyriformis toxicity	0.39	0.563	0.794	0.285
Minnow toxicity	2.341	2.337	1.603	4.394

Table 3. ADMET properties of the selected bioactive compounds.

Molecular descriptors	Esculetin	Aloe emodin	Chrysophanic acid	Aloesin
Molecular weight	178.143	270.24	254.241	394.376
LogP	1.2042	1.3655	2.18162	−0.54658
#Rotatable bonds	0	1	0	4
#Acceptors	4	5	4	9
#Donors	2	3	2	5
Surface area	72.668	113.283	108.489	158.969

Table 4. Molecular descriptors of the selected bioactive compounds. # = Number of

esculetin was predicted to be a CYP2C9 substrate, implying that it may be metabolised by this enzyme without exhibiting inhibitory effects[57]. In addition to the CYP enzymes, we also assessed the involvement of the breast cancer resistance protein (BCRP), which plays a critical role in drug efflux and multidrug resistance[58,59]. Aloe emodin and chrysophanic acid were predicted to be BCRP inhibitors, albeit with low confidence. If validated experimentally, this suggests they may interfere with BCRP-mediated drug transport, potentially altering the pharmacokinetics of BCRP substrates[58,59]. In contrast, esculetin and aloesin were confidently predicted to be non-inhibitors, reducing concerns about efflux-related interactions. Furthermore, none of the compounds were predicted to inhibit OATP1B1 or OATP1B3, which are hepatic uptake transporters important for drug clearance.

The lack of interaction with these transporters suggests that hepatic accumulation or altered drug disposition via this route is unlikely[60,61]. Overall, esculetin and aloesin, given their metabolically favourable profiles, appear to be safer candidates for further evaluation.

The predicted excretion parameter showed that total clearance ranged from 0.008 to 0.671 for the ligands, while all the ligands and control were not substrates for renal OCT2. Clearance values (0.008 to 0.671) suggest varying elimination rates, with no renal OCT2 interactions[62]. Ames's toxicity profiling of the ligands showed that all the ligands, apart from aloe emodin and chrysophanic acid, were not toxic. Hepatotoxicity for both ligands and the control showed that all were not toxic except for aloesin. Molecular weight of the ligands ranged from 178.143 to 394.376. The log P values ranged from − 0.54658 to 2.18162, while the number of rotatable bonds ranged from 0 to 4. On the other hand, the number of acceptors and donors ranged from 4 to 9 and 2–5. The surface area of the bioactive area ranged from 72.668 to 158.969.

Toxicity profiling showed that aloe emodin and chrysophanic acid were mutagenic[63], while aloesin was hepatotoxic. Molecular descriptors confirm drug-likeness, with molecular weights (178.143–394.376 Da), logP (−0.54658 to 2.18162), and hydrogen bond properties within acceptable ranges of the Lipinski rule of five[36,37]. Their compliance with the Lipinski rule of five indicates that they could serve as potential oral drugs. Furthermore, these findings suggest esculetin and aloe emodin have the most promising pharmacokinetic profiles, but toxicity concerns warrant further evaluation.

Density function theory

To further assess chemical reactivity, regioselectivity, stereoselectivity, and the interactions between reacting orbitals in order to determine the relative reactivity and chemical behaviour of the species, frontier molecular orbital (FMO) theory was carried out as reported previously[64–66]. For all the ligands, we looked at the global hardness (η), orbital overlap (π), softness (S), electrophilicity index (ω), and chemical potential (μ) of certain molecules (Supplementary Fig. 1 and Table 1). The energy gap (ΔE) of the ligands was found to be between 0.0839 eV (CID 5281416) and 0.3184 eV (control). LIGAND 160,190 had the smallest energy gap. Lower ΔE values suggest higher reactivity, while higher values indicate greater stability, implying that the test ligands were more reactive than the control. Notably, CID 5281416 exhibits the highest electrophilicity index (ω = 0.472791 eV), implying a strong potential to accept electrons. The lower energy gap reported for esculetin and high electrophilicity suggest significant reactivity, making it a potential candidate for biological interactions[67]. The other ligands, CIDs 10207, 160190, and 10,08, exhibit moderate reactivity with ΔE values between approximately 0.2696 eV and 0.2894 eV, indicating a balance between stability and reactivity. The control compound's higher ΔE suggests it is the most stable and least reactive among the group; however, in the presence of the target protein, the bioactive compound was also stable as discussed earlier.

Conclusion

This study provides insights into the potential inhibitory activity of selected phytoconstituents against *H. pylori* neutrophil-activating protein (NAP). Molecular docking revealed that aloesin exhibited the highest binding affinity (−7.4 kcal/mol), followed by aloe-emodin and chrysophanic acid (−6.4 kcal/mol), and esculetin (−6.3 kcal/mol), all outperforming the control ligand (−4.3 kcal/mol). Key receptor-ligand interactions involved Ser135, Glu46, and Tyr99, contributing to complex stability. Molecular dynamics simulations confirmed ligand-protein stability, with RMSD values within an acceptable range (≤ 4 Å). The ranking of the ligands in terms of docking scores and RMSD values revealed that chrysophanic acid and esculetin possessed strong binding affinities combined with high dynamic stability, making them the best leading compounds. Our RMSF analysis highlighted fluctuations at residues 30, 80/85, and 140, while contact analysis emphasized the role of water bridges and hydrogen bonds in stabilization. Overall, the compounds induced conformational perturbations that can induce conformational changes that disrupt NAP function, they could serve as potential inhibitors, reducing *H. pylori*-mediated ulcerogenesis. ADMET prediction showed favourable pharmacokinetics for all the ligands except for aloesin that showed hepatotoxicity, while their low energy gaps indicate good biological activities. These findings suggest aloesin and related phytochemicals as promising candidates for *H. pylori* treatment. Future in vitro and in vivo studies are needed to validate their therapeutic potential for ulcer management.

Data availability

Data is provided within the manuscript or supplementary information files.

Received: 26 February 2025; Accepted: 21 November 2025
Published online: 29 November 2025

References

1. Gravina, A. G. et al. *Helicobacter pylori* and extragastric diseases: A review. *World J. Gastroenterol.* **24** (29), 3204–3221. https://doi.org/10.3748/wjg.v24.i29.3204 (2018).
2. Ahmed, K. S. et al. Prevalence study to elucidate the transmission pathways of Helicobacter pylori at oral and gastroduodenal sites of a South Indian population. *Singapore Med. J.* **47** (4), 291–296 (2006).
3. Elbehiry, A. et al. Helicobacter pylori infection: current status and future prospects on Diagnostic, therapeutic and control challenges. *Antibiot. (Basel Switzerland).* **12** (2), 191. https://doi.org/10.3390/antibiotics12020191 (2023).
4. Codolo, G., Coletta, S., D'Elios, M. M. & de Bernard, M. HP-NAP of Helicobacter pylori: the power of the Immunomodulation. *Front. Immunol.* **13**, 944139. https://doi.org/10.3389/fimmu.2022.944139 (2022).
5. Fu, H. W. & Lai, Y. C. The role of Helicobacter pylori Neutrophil-Activating protein in the pathogenesis of H. pylori and beyond: from a virulence factor to therapeutic targets and therapeutic agents. *Int. J. Mol. Sci.* **24** (1), 91. https://doi.org/10.3390/ijms24010091 (2022).

6. Kamada, T. et al. Evidence-based clinical practice guidelines for peptic ulcer disease 2020. *J. Gastroenterol.* **56** (4), 303–322. https://doi.org/10.1007/s00535-021-01769-0 (2021).
7. Vomero, N. D. & Colpo, E. Nutritional care in peptic ulcer. Arquivos brasileiros de cirurgia digestiva: ABCD = Brazilian archives of digestive surgery. *ABCD Brazilian Archives Dig. Sur.* **27**(4), 298–302. https://doi.org/10.1590/S0102-67202014000400017 (2014).
8. Nestegard, O. et al. Helicobacter pylori resistance to antibiotics before and after treatment: incidence of eradication failure. *PloS One*. **17** (4), e0265322. https://doi.org/10.1371/journal.pone.0265322 (2022).
9. Tran, V. H. et al. Current status of Helicobacter pylori resistance to clarithromycin and Levofloxacin in vietnam: results from molecular analysis of gastric biopsy specimens. *J. Global Antimicrob. Resist.* **36**, 76–82. https://doi.org/10.1016/j.jgar.2023.12.026 (2024).
10. Shao, Y. et al. Analysis of Helicobacter pylori resistance in patients with different gastric diseases. *Sci. Rep.* **14** (1), 4912. https://doi.org/10.1038/s41598-024-55589-2 (2024).
11. Olmedo, L. et al. Evolution of the use, effectiveness and safety of bismuth-containing quadruple therapy for Helicobacter pylori infection between 2013 and 2021: results from the European registry on H. pylori management (Hp-EuReg). *Gut* **74** (1), 15–25. https://doi.org/10.1136/gutjnl-2024-332804 (2024). … Hp-EuReg investigators*.
12. Yang, E. H. et al. 10-Day versus 14-day bismuth quadruple therapy for first-line eradication of *Helicobacter pylori* infection: a randomised, open-label, non-inferiority trial. *EClinicalMedicine* **70**, 102529. https://doi.org/10.1016/j.eclinm.2024.102529 (2024).
13. Ahmed, S. K. et al. Antimicrobial resistance: Impacts, challenges, and future prospects. *J. Med. Surg. Public. Health*. **2**, 100081. https://doi.org/10.1016/j.glmedi.2024.100081 (2024).
14. Guerra-Valle, M., Orellana-Palma, P. & Petzold, G. Plant-Based polyphenols: Anti-*Helicobacter pylori* effect and improvement of gut microbiota. *Antioxid. (Basel Switzerland)*. **11** (1), 109. https://doi.org/10.3390/antiox11010109 (2022).
15. Deng, R., Chen, X., Zhao, S., Zhang, Q. & Shi, Y. The effects and mechanisms of natural products on Helicobacter pylori eradication. *Front. Cell. Infect. Microbiol.* **14**, 1360852. https://doi.org/10.3389/fcimb.2024.1360852 (2024).
16. Hęś, M., Dziedzic, K., Górecka, D., Jędrusek-Golińska, A. & Gujska, E. *Aloe vera* (L.) Webb.: natural sources of antioxidants–a review. *Plant Foods Hum. Nutr.* **74**(3), 255–265 (2019).
17. Ray, A., Gupta, S. D. & Ghosh, S. Evaluation of anti-oxidative activity and UV absorption potential of the extracts of *Aloe vera* L. gel from different growth periods of plants. *Ind. Crops Prod.* **49**, 712–719 (2013).
18. Nejatzadeh-Barandozi, F. Antibacterial activities and antioxidant capacity of *Aloe vera*. *Org. Med. Chem. Lett.* **3**(1), 5. https://doi.org/10.1186/2191-2858-3-5 (2013).
19. Svitina, H., Hamman, J. H. & Gouws, C. Molecular mechanisms and associated cell signalling pathways underlying the anticancer properties of phytochemical compounds from Aloe species. *Exp. Therap. Med.* **22**(2), 852. https://doi.org/10.3892/etm.2021.10284 (2021).
20. Sánchez, M., González-Burgos, E., Iglesias, I. & Gómez-Serranillos, M. P. Pharmacological update properties of *Aloe vera* and its major active constituents. *Molecules* **25**(6), 1324. https://doi.org/10.3390/molecules25061324 (2020).
21. Zhao, Y., Chen, Z., Cai, Y., Xue, J., Zhang, L., Wang, L., … Sun, Y. (2024). Aloe-emodin destroys the biofilm of Helicobacter pylori by targeting the outer membrane protein 6. Microbiological Research, 278, 127539. https://doi.org/10.1016/j.micres.2023.127539.
22. Ranjith, D. Molecular Docking studies of *Aloe vera* for their potential antibacterial activity using Argus lab 4.0. 1. *Pharma Innov. J.* **8**, 481–487 (2019).
23. Li, T., Lu, Y., Zhang, H., Wang, L., Beier, R. C., Jin, Y., … Hou, X. (2021). Antibacterial activity and membrane-targeting mechanism of aloe-emodin against Staphylococcus epidermidis.*Frontiers in Microbiology*, *12*, 621866. https://doi.org/10.3389/fmicb.2021.621866.
24. Zanotti, G. et al. Structure of the neutrophil-activating protein from Helicobacter pylori. *J. Mol. Biol.* **323** (1), 125–130. https://doi.org/10.1016/s0022-2836(02)00879-3 (2002).
25. Cousins, K. R. *ChemDraw Ultra 9.0. CambridgeSoft, 100 CambridgePark Drive, Cambridge, MA 02140. www.cambridgesoft.com* (See Web site for pricing options, 2005).
26. Jejurikar, B. L. & Rohane, S. H. Drug designing in discovery studio. (2021)
27. Kubra, B. et al. Inhibition of the predicted allosteric site of the SARS-CoV-2 main protease through flavonoids. *J. Biomol. Struct. Dynamics*. **41** (18), 9103–9120. https://doi.org/10.1080/07391102.2022.2140201 (2023).
28. Abdalla, M., Abdelkhalig, S. M., Edet, U. O., Zothantluanga, J. H., Umoh, E. A., Moglad,E., … Al-Shouli, S. (2024). Molecular dynamics-based computational investigations on the influence of tumor suppressor p53 binding protein against other proteins/peptides.Scientific reports, 14(1), 29871. https://doi.org/10.1038/s41598-024-81499-4.
29. Edet, U. O. et al. Antimicrobial analysis of honey against Staphylococcus aureus isolates from wound, ADMET properties of its bioactive compounds and in-silico evaluation against dihydropteroate synthase. *BMC Complement. Med. Ther.* **23** (1), 39. https://doi.org/10.1186/s12906-023-03841-z (2023).
30. Bebia, G. P., Edet, U. O., Eyo, A. A. O., Ugwu, J. C., Mbim, E. N., Ogba, O. M., …Nwaokorie, F. O. (2024). Evaluation of bioactive compounds in Tetrapleura tetraptera(uyayak) and its activity against dihydropteroate synthase (1AJ2) of E. coli: in-sight from ADMET profiling and molecular docking. Natural Product Communications, 19(10), 1934578X241284045. https://doi.org/10.1177/1934578X2412840.
31. Edet, U. O. et al. Evaluation of Annona muricata extract against Staphylococcus aureus isolate and in-silico activity of bioactive compounds against capsular protein (Cap5O). *BMC Complement. Med. Ther.* **22** (1), 192. https://doi.org/10.1186/s12906-022-03672-4 (2022).
32. Maliehe, T. S. et al. Chemical profile, antioxidant and antibacterial activities, mechanisms of action of the leaf extract of aloe arborescens mill. *Plants* **12**(4), 869. https://doi.org/10.3390/plants12040869 (2023).
33. Eberhardt, J., Santos-Martins, D., Tillack, A. F. & Forli, S. AutoDock Vina 1.2. 0: new Docking methods, expanded force field, and python bindings. *J. Chem. Inf. Model.* **61** (8), 3891–3898 (2021).
34. Deghady, A. M., Hussein, R. K., Alhamzani, A. G. & Mera, A. Density functional theory and molecular Docking investigations of the chemical and antibacterial activities for 1-(4-Hydroxyphenyl)-3-phenylprop-2-en-1-one. *Molecules* **26** (12), 3631. https://doi.org/10.3390/molecules26123631 (2021).
35. Pires, D. E., Blundell, T. L. & Ascher, D. B. PkCSM: predicting small-molecule Pharmacokinetic and toxicity properties using graph-based signatures. *J. Med. Chem.* **58** (9), 4066–4072 (2015).
36. Lipinski, C. A. Lead-and drug-like compounds: the rule-of-five revolution. *Drug Discovery Today: Technol.* **1** (4), 337–341 (2004).
37. Veber, D. F. et al. Molecular properties that influence the oral bioavailability of drug candidates. *J. Med. Chem.* **45** (12), 2615–2623. https://doi.org/10.1021/jm020017n (2002).
38. Alsedfy, M. Y., Ebnalwaled, A. A., Moustafa, M. & Said, A. H. Investigating the binding affinity, molecular dynamics, and ADMET properties of curcumin-IONPs as a mucoadhesive bioavailable oral treatment for iron deficiency anemia. *Sci. Rep.* **14** (1), 22027. https://doi.org/10.1038/s41598-024-72577-8 (2024).
39. Kushwaha, P. P. et al. Identification of natural inhibitors against SARS-CoV-2 drugable targets using molecular Docking, molecular dynamics Simulation, and MM-PBSA approach. *Front. Cell. Infect. Microbiol.* **11**, 730288. https://doi.org/10.3389/fcimb.2021.730288 (2021).
40. Adegoke, O. A., Ghosh, M. & Mukherjee, A. Spectrophotometric and thermodynamic studies of the interactions of 4-carboxyl-2,6-dinitrophenylazohydroxynaphthalenes with bovine serum albumin. *Spectrochim. Acta A*. **96**, 1038–1046. https://doi.org/10.1016/j.saa.2012.08.014 (2012).

41. Nwaokorie, F., Abdalla, M., Edet, U. O., Abdalla, A. M., Okpo, E. A., Shami, A.,… Alaribe, S. C. (2024). In-silico assessment of bioactive compounds from chewing stick (Salvadora Persica) against N-acetylneuraminate lyase (5ZKA) of Fusobacterium nucleatum involved in salicyclic acid metabolism. *Journal of Molecular Structure*, *1316*, 138733.https://doi.org/10.1016/j.molstruc.2024.138733.
42. Kufareva, I. & Abagyan, R. Methods of protein structure comparison. In *Homology Modeling: Methods and Protocols* 231–257 (Humana, 2012).
43. Ceci, P., Mangiarotti, L., Rivetti, C. & Chiancone, E. The neutrophil-activating Dps protein of Helicobacter pylori, HP-NAP, adopts a mechanism different from Escherichia coli Dps to bind and condense DNA. *Nucleic Acids Res.* **35** (7), 2247–2256. https://doi.org/10.1093/nar/gkm077 (2007).
44. Sharma, J. et al. An in-silico evaluation of different bioactive molecules of tea for their Inhibition potency against Non structural protein-15 of SARS-CoV-2. *Food Chem.* **346**, 128933. https://doi.org/10.1016/j.foodchem.2020.128933 (2021).
45. Zaman, N. et al. Dynamics of water-mediated interaction effects on the stability and transmission of Omicron. *Sci. Rep.* **13** (1), 20894. https://doi.org/10.1038/s41598-023-48186-2 (2023).
46. Herrington, N. B. & Kellogg, G. E. 3D interaction homology: computational Titration of aspartic acid, glutamic acid and histidine can create pH-tunable hydropathic environment maps. *Front. Mol. Biosci.* **8**, 773385. https://doi.org/10.3389/fmolb.2021.773385 (2021).
47. Polgár, L. The catalytic triad of Serine peptidases. *Cell. Mol. Life Sci.* **62** (19–20), 2161–2172. https://doi.org/10.1007/s00018-005-5192-5 (2005).
48. Pyrkov, T. V., Pyrkova, D. V., Balitskaya, E. D. & Efremov, R. G. The role of stacking interactions in complexes of proteins with adenine and guanine fragments of ligands. *Acta Naturae (англоязычная версия)*. **1** (1 (1)), 124–127 (2009).
49. Wang, J. & Hou, T. Recent advances on aqueous solubility prediction. *Comb. Chem. High. Throughput Screen.* **14** (5), 328–338. https://doi.org/10.2174/138620711795508331 (2011).
50. Oftadeh, M., Mahani, N. M. & Hamadanian, M. Density functional theory study of the local molecular properties of acetamide derivatives as anti-HIV drugs. *Res. Pharm. Sci.* **8** (4), 285 (2013).
51. Simonin, A., Montalbetti, N., Gyimesi, G., Pujol-Giménez, J. & Hediger, M. A. The hydroxyl side chain of a highly conserved Serine residue is required for cation selectivity and substrate transport in the glial glutamate transporter GLT-1/SLC1A2. *J. Biol. Chem.* **290** (51), 30464–30474. https://doi.org/10.1074/jbc.M115.689836 (2015).
52. Rampogu, S., Lee, G., Park, J. S., Lee, K. W. & Kim, M. O. Molecular Docking and molecular dynamics simulations discover Curcumin analogue as a plausible dual inhibitor for SARS-CoV-2. *Int. J. Mol. Sci.* **23** (3), 1771. https://doi.org/10.3390/ijms23031771 (2022).
53. Shirali, A. et al. A comprehensive survey of scoring functions for protein Docking models. *BMC Bioinform.* **26** (1), 25. https://doi.org/10.1186/s12859-024-05991-4 (2025).
54. Avdeef, A. *Absorption and Drug Development: solubility, permeability, and Charge State* (Wiley, 2012).
55. Parthasarathy, S., Aly, S. H., Tharumasivam, S. V., Giridharan, B., Chandran, J.,Thirumurthy, P., … El-Shazly, M. (2025). Unlocking nature's secrets: a review on the pharmacokinetics of plant-based medicines and herbal remedies. *Natural Product Research*, 1–25.
56. Deodhar, M. et al. Mechanisms of CYP450 Inhibition: Understanding drug-drug interactions due to mechanism-based Inhibition in clinical practice. *Pharmaceutics* **12** (9), 846 (2020).
57. Rendic, S. & Guengerich, F. P. Survey of human oxidoreductases and cytochrome P450 enzymes involved in the metabolism of xenobiotic and natural chemicals. *Chem. Res. Toxicol.* **28** (1), 38–42 (2015).
58. Mao, Q. & Unadkat, J. D. Role of the breast cancer resistance protein (BCRP/ABCG2) in drug transport—an update. *AAPS J.* **17** (1), 65–82 (2015).
59. Robey, R. W. et al. Revisiting the role of efflux pumps in multidrug-resistant cancer. *Nat. Rev. Cancer*. **18** (7), 452 (2018).
60. Garrison, D. A., Talebi, Z., Eisenmann, E. D., Sparreboom, A. & Baker, S. D. Role of OATP1B1 and OATP1B3 in drug-drug interactions mediated by tyrosine kinase inhibitors. *Pharmaceutics* **12** (9), 856 (2020).
61. Shitara, Y. et al. Clinical significance of organic anion transporting polypeptides (OATPs) in drug disposition: their roles in hepatic clearance and intestinal absorption. *Biopharm. Drug Dispos.* **34** (1), 45–78 (2013).
62. El-Kattan, A. & Varma, M. Oral absorption, intestinal metabolism and human oral bioavailability. *Top. Drug Metabolism*. **10**, 31087. https://doi.org/10.5772/31087 (2012).
63. Zanger, U. M. & Schwab, M. Cytochrome P450 enzymes in drug metabolism: regulation of gene expression, enzyme activities, and impact of genetic variation. *Pharmacol. Ther.* **138**(1), 103–141. https://doi.org/10.1016/j.pharmthera.2012.12.007 (2013).
64. Tang, S., Wang, B., Liu, X., Xi, W., Yue, Y., Tan, X., … Huang, L. (2025). Structural insights and biological activities of flavonoids: Implications for novel applications.Food Frontiers, 6(1), 218–247.https://doi.org/10.1002/fft2.494.
65. Guengerich, F. P. Roles of individual human cytochrome P450 enzymes in drug metabolism. *Pharmacol. Rev.* **76** (6), 1104–1132. https://doi.org/10.1124/pharmrev.124.001173 (2024).
66. Galetin, A., Brouwer, K. L. R., Tweedie, D., Yoshida, K., Sjöstedt, N., Aleksunes,L., Chu, X., Evers, R., Hafey, M. J., Lai, Y., Matsson, P., Riselli, A., Shen, H.,Sparreboom, A., Varma, M. V. S., Yang, J., Yang, X., Yee, S. W., Zamek-Gliszczynski,M. J., Zhang, L., … Giacomini, K. M. (2024). Membrane transporters in drug development and as determinants of precision medicine. Nature reviews. Drug discovery, 23(4), 255–280. https://doi.org/10.1038/s41573-023-00877-1.
67. Guo, X. et al. In vitro investigation of the mutagenic potential of *Aloe vera* extracts. *Toxicol. Res.* **3**(6), 487–496. https://doi.org/10.1039/c4tx00053f (2014).

Author contributions

Conceptualisation: U.O.E., E.E.I., and M.A.; methodology, U.O.E., E.E.I., W.A.E. and G.B.; writing—original draft preparation, U.O.E., E.E.I., M.E.A., and A.E.; writing—review and editing, U.O.E., E.E.I., and R.M.A.; visualization, B.E. and F.N.

Declarations

Competing interests

The authors declare no competing interests.

Additional information

Supplementary Information The online version contains supplementary material available at https://doi.org/10.1038/s41598-025-30119-w.

Correspondence and requests for materials should be addressed to U.O.E. or M.A.

Reprints and permissions information is available at www.nature.com/reprints.